Applied Microbiology and Biotechnology (2022) 106:1127–1137
https://doi.org/10.1007/s00253-022-11779-4

BIOTECHNOLOGICAL PRODUCTS AND PROCESS ENGINEERING

Biosynthesis and applications of iron oxide nanocomposites synthesized by recombinant *Escherichia coli*

Jae Hwan Jung[1] · Minkyung Cho[2] · Tae Seok Seo[3] · Sang Yup Lee[2,4]

Received: 22 September 2021 / Revised: 11 January 2022 / Accepted: 13 January 2022 / Published online: 21 January 2022

Abstract

Recombinant *Escherichia coli* (*E. coli*) strain that produces phytochelatin (PC) and/or metallothionein (MT) can synthesize various metal nanoparticles (NPs) by reducing metal ions. Here we report in vivo biosynthesis of iron oxide nanocomposites (NCs) using recombinant *E. coli*. We designed a strategy of biosynthesizing iron oxide NCs by first internalizing chemically synthesized iron oxide NPs, followed by the reduction of added metal ions on the surface of internalized NPs by PC and/or MT in *E. coli*. For this, chemically synthesized Fe_3O_4 NPs were internalized by recombinant *E. coli*, and then, Au and Ag ions were added for the biosynthesis of $AuFe_3O_4$ and $AgFe_3O_4$ NCs, respectively. The NCs synthesized were analyzed by transmission electron microscopy, UV–vis spectrophotometry, and X-ray diffractometry to characterize their shape, optical property, and crystallinity. The Fe_3O_4 NPs in the biosynthesized NCs allowed easy purification of the biosynthesized NCs by applying a magnetic field. The $AuFe_3O_4$ NCs were used for enzyme-linked immunosorbent assay to detect prostate-specific antigen protein, while $AgFe_3O_4$ NCs were utilized for the antimicrobial application with low minimum inhibitory concentration. As recombinant *E. coli* can uptake and reduce various NPs and metal ions, biosynthesis of a wide range of NCs as new nanomaterials will be possible for diverse applications.

Key points

- *$AuFe_3O_4$ and $AgFe_3O_4$ nanocomposites were synthesized by recombinant E. coli.*
- *Escherichia coli synthesized different iron oxide NCs depending on the metal ions to be added.*
- *Biosynthesized $AuFe_3O_4$ NC was used for ELISA and $AgFe_3O_4$ NC for antimicrobial tests.*

Keywords Biosynthesis · Recombinant *Escherichia coli* · Nanocomposite · Biosensor · Antimicrobial activity

Introduction

Metal nanomaterials have been explored for diverse applications such as catalytic reaction, medical imaging, biosensors, and biomedical therapy due to their unique physical and chemical properties (Choi and Lee 2020; Choi et al. 2018a, b; Jeong et al. 2018; Yu et al. 2016; Zhang et al. 2018). However, metal nanomaterials have traditionally manufactured under rather harsh reaction conditions such as high temperature in multiple and complicated reaction steps involving

✉ Jae Hwan Jung
jjaehwan@dankook.ac.kr

✉ Tae Seok Seo
seots@khu.ac.kr

[1] Department of Pharmaceutical Engineering, Dankook University, 119 Dandae-ro, Dongnam-gu, Cheonan-si 31116, Republic of Korea

[2] Department of Chemical and Biomolecular Engineering, Korea Advanced Institute of Science and Technology (KAIST), 291 Daehak-ro, Yuseong-gu, Daejeon 34141, Republic of Korea

[3] Department of Chemical Engineering (BK21 FOUR Integrated Engineering Program), Kyung Hee University, 1 Seochon-dong, Giheung-gu, Yongin-si, Gyeonggi-do 17140, Republic of Korea

[4] Metabolic and Biomolecular Engineering National Research Laboratory, Systems Metabolic Engineering and Systems Healthcare (SMESH) Laboratory, Department of Chemical and Biomolecular Engineering (BK21 Plus Program), BioProcess Engineering Research Center and Institute for the BioCentury, Korea Advanced Institute of Science and Technology (KAIST), 291 Daehak-ro, Yuseong-gu, Daejeon 34141, Republic of Korea

toxic chemicals. To overcome such problems, the biosynthesis of metal nanomaterials has been attracting much attention. Between the in vivo and in vitro biosynthesis methods, the former is more advantageous because it does not require cell lysis and can provide enough reducing power for the biosynthesis of metal nanomaterials. We recently reported that in vivo biosynthesis of metal nanomaterials in recombinant *E. coli* cells provides a 3.5-fold higher reducing power than in vitro method (Choi et al. 2018a, b). So far, most metal nanomaterials biosynthesized have been single element nanomaterials, but multi-element nanomaterial biosynthesis is also being actively pursued (Choi and Lee 2020). We recently reported biosynthesis of highly ordered core–shell NC of Au nanorod (NR)-Ag in recombinant *E. coli* expressing the *Pseudomonas putida mt* and *Arabidopsis thaliana pcs* genes encoding metallothionein (MT) and phytochelatin synthase (PCS) synthesizing phytochelatin (PC), respectively (Park et al. 2010; Jung et al. 2012, 2018). However, there has been a great need for biosynthesizing more diverse metal NCs for various applications.

In this study, we report a new strategy for the biosynthesis of metal NCs. First, chemically synthesized Fe_3O_4 NPs are internalized into the *E. coli*. Then, the desired metal ions (Au and Ag in this study) are added for their reduction and growth on the surface of Fe_3O_4 NPs by MT and PC, thereby synthesizing the NCs. The biosynthesized $AuFe_3O_4$ and $AgFe_3O_4$ NCs were analyzed by transmission electron microscopy (TEM), X-ray diffractometry (XRD), and UV/Vis spectrophotometry after easy purification from the cells by applying a magnetic field. Finally, the biosynthesized $AuFe_3O_4$ and $AgFe_3O_4$ NCs were employed for enzyme-linked immunosorbent assay (ELISA) to detect prostate-specific antigens and antimicrobial applications, respectively.

Materials and methods

Materials

For biosynthesis of the $AuFe_3O_4$ and $AgFe_3O_4$ NCs, an LB broth (high salt, LPS SOLUTION), gold (III) chloride trihydrate ($HAuCl_4 \bullet 3H_2O$, ≥ 49.0% Au basis, Sigma-Aldrich), a silver nitrate solution ($AgNO_3$, 0.01 M, Fluka), and Fe_3O_4 NP (10–15 nm, SkySpring Nanomaterials) were used. For isolation of the $AuFe_3O_4$ and $AgFe_3O_4$ NCs, a B-PER bacterial protein extraction solution (Thermo Scientific), lysozyme (50 mg/mL, Sigma-Aldrich), DL-dithiothreitol (≥ 98%; TLC, ≥ 99%; titration, Sigma), proteinase K (> 800 units/mL, Sigma), Triton X-100 (Sigma), sodium dodecyl sulfate (≥ 99.0%; GC, Fluka) were employed. Ampicillin, isopropyl-β-D-thiogalactopyranoside (IPTG), a human PSA-total ELISA kit, prostate-specific antigen (PSA) from human semen, C reactive protein (CRP) from human plasma, and chorionic gonadotropin human (hCG) were obtained from Sigma-Aldrich. A Mueller Hinton broth was ordered from DIFCO for the antimicrobial test.

In vivo biosynthesis of the Fe_3O_4 NCs

$AuFe_3O_4$ and $AgFe_3O_4$ NCs were biosynthesized by employing recombinant *E. coli* DH5α strains harboring pTJ1-AtPCS, pTJ1-PpMT, pACtac-PpMT, and pTJ1-PpMT-n-AtPCS, either alone or together (Park et al. 2010). One hundred microliter of the recombinant *E. coli* were incubated in 10 mL of an LB broth medium including ampicillin (50 μg/mL) for 18 h at 37 °C with 200 rpm in a shaking incubator. Then, 1 mL of the incubated *E. coli* was subcultured in 100 mL of a fresh LB broth medium for 2 h 30 min at 37 °C with 200 rpm. After incubation, the cultured *E. coli* were measured by a UV/Vis spectrophotometer (UV-2450, SHIMADZU) to check the absorbance of the cell solution at 600 nm, OD_{600}. Then, 100 μL of IPTG was added to 100 mL of the cell solution to get 1 mM final concentration, and the solution was incubated at 37 °C with 200 rpm for 90 min. Fifty milliliters of Fe_3O_4 NP solution (12 μg/mL) in a phosphate-buffered saline (PBS) was added to the same volume of the *E. coli* solution. During 5-h incubation, Fe_3O_4 NPs were internalized into the *E. coli* (Cui et al. 2012; Jung et al. 2018). Then, 10 mM of gold (III) chloride trihydrate and a silver nitrate solution were added to the cell solution, respectively. The final Au concentration in the cell solution was from 0.25, 0.5, and 0.75 to 1 mM, and the final Ag concentration was from 0.5, 1, and 1.5 to 2 mM. Then, the recombinant *E. coli* and metal ions were incubated at 37 °C at 200 rpm for 48 h.

Isolation of the Fe_3O_4 NCs

When the biosynthesis was complete, 10 mL of the *E. coli* solution containing the NCs were aliquoted to 15-mL conical tubes and then washed with PBS buffer three times by centrifugation at 3500 rpm 5 min. To lyse the cell wall, 4 mL of a B-PER bacterial protein extraction solution and 8 μL of lysozyme were added to each aliquot and incubated at room temperature for 1 h with gentle mixing. After centrifugation at 4000 rpm for 5 min, lysed cell complexes, including the NCs, were washed three times with PBS. For further digestion of protein-NC complexes, 2 mL of a denaturing solution consisting of 8 M urea, 20 mM DL-dithiothreitol, and 1 M β-mercaptoethanol were used. The mixture was incubated overnight at room temperature. After washing three times with DI water, the NC complexes were re-suspended in a 1 mL proteinase mixture including 20 μL of proteinase K, 20 μL of Triton X-100,

and 20 mg of sodium dodecyl sulfate, and incubated at 37 °C for 1 day. Then, the NCs were isolated by applying an external magnet to collect only magnetic materials and stored in DI water at 4 °C before use.

Protein detection using the $AuFe_3O_4$ NCs

We carried out ELISA for PSA detection by using the $AuFe_3O_4$ NC and a PSA ELISA kit. All the solutions were prepared by the kit manufacturer's protocol. For the synthesis of "detection anti-PSA" conjugated the $AuFe_3O_4$ NCs, 0.8 g of the $AuFe_3O_4$ NCs was incubated with 20 µL of detection antibody concentrate (anti-PSA, RAB0331, Sigma-Aldrich) in 380 µL of PBS overnight. In the test, we used the $AuFe_3O_4$ NCs biosynthesized with 2 mM Au. The target protein PSA (100 ng/mL), non-target proteins CRP (100 mg/L) and hCG (100 mIU/mL), and control 1X PBS buffer (each 100 µL volume) were added to the "capture anti-PSA" coated well plate and incubated at room temperature with gentle mixing for 2 h 30 min. After washing the wells with a washing buffer, 100 µL of the "detection anti-PSA" conjugating the $AuFe_3O_4$ NC was added and incubated at room temperature with gentle shaking for 2 h. Then, 100 µL of a tetramethylbenzidine (TMB) reagent was added to each well and incubated at room temperature for 6 h. All the reactions were performed in triplicate.

Antimicrobial application using the $AgFe_3O_4$ NCs

The minimum inhibitory concentration (MIC) of the $AgFe_3O_4$ NC was measured with 2 g of gram-positive bacteria, *Staphylococcus aureus* (ATCC 12,600) and *Listeria monocytogenes* (ATCC 15,313), and 1 g Gram-negative bacteria, *Salmonella enterica* (ATCC 14,028). In the test, we used the $AgFe_3O_4$ NC biosynthesized with 2 mM Ag. We verified the MIC value of the NCs inhibiting the visible growth of bacteria with incubation at 37 °C for 1 day. The antimicrobial test was carried out on a 96-well microtitration plate for a triplicate test with each bacterium. Before the test, all three bacteria were grown in a Mueller Hinton Broth medium at 37 °C for 18 h and diluted to 10^6 cells/mL. Then, 100 µL of the bacteria solution was added to the well plates. The final concentration of the $AgFe_3O_4$ NCs in each well was from 0, 0.07, 0.14, 0.28, 0.56, and 1.12, to 2.24 mg/L.

Characterization of the biosynthesized NCs

The recombinant *E. coli* containing the NCs and the purified NCs were characterized by a field emission transmission electron microscope (FE-TEM, Tecnai G^2 F30 S-Twin, FEI) operated at a voltage of 300 kV. The size of Au NPs was measured based on the TEM images. Mean and standard deviation of mean were calculated from the data obtained from at least twenty objects. An inductively coupled plasma-mass spectrometer (ICP-MS, Agilent ICP-MS 7700S, Agilent) was used to obtain the mass ratio of the NCs and their content. In addition, the NCs were characterized by a UV/Vis spectrophotometer (UV-2450, SHIMADZU) and a multi-purpose thin-film X-ray diffractometer (MPA-XRD, D/MAX-2500, Rigaku). All the measurements were performed with at least three replicate samples.

Results

In vivo biosynthesis of the NCs

Au and Ag ions were added to the recombinant *E. coli* internalized Fe_3O_4 NPs (10–15 nm diameter) to biosynthesize the $AuFe_3O_4$ and $AgFe_3O_4$ NCs. After the biosynthesis, the *E. coli* were collected by centrifugation and isolated by applying an external magnet. Transmission electron microscopy (TEM) was utilized to confirm the NCs biosynthesized inside the *E. coli* (Fig. 1), and the original *E. coli* were also analyzed as a negative control (Fig. S1). Here, we hypothesized that the *E. coli* isolated by the magnet contained $AuFe_3O_4$ and $AgFe_3O_4$ NCs biosynthesized inside. In the images, Au and Ag NPs of the NCs in *E. coli* were shown as spherical (Fig. 1a and b). In the magnified TEM image of the $AuFe_3O_4$ NCs (Fig. 1c), a dark popcorn-shaped particle (around 90-nm diameter), an Au NP, was found. The shape of the particle was similar to the typical Au NPs biosynthesized (Park et al. 2010). In the TEM image of the $AgFe_3O_4$ NCs, many spherical biosynthesized Ag NPs (around 40-nm diameter) were shown (Fig. 1d). On the other hand, the Fe_3O_4 NPs were not seen even in the magnified TEM images, even though the *E. coli* were isolated and purified by external magnets (Fig. 1c and d). Hence, an energy-dispersive X-ray (EDX) was utilized to identify the component of the NCs inside the *E. coli*. As a result, Fe, Au, and Ag were identified, respectively (Fig. 1e and f), confirming that the $AuFe_3O_4$ or $AgFe_3O_4$ NCs were successfully biosynthesized from recombinant *E. coli*.

Isolation of the NCs

The recombinant *E. coli* containing chemically synthesized Fe_3O_4 NPs and the biosynthesized $AuFe_3O_4$ and $AgFe_3O_4$ NCs were isolated from a medium by centrifugation (Fig. 2). The color of the cell pellets was different depending on the nanomaterials. The control *E. coli* exhibited bright brown color (Fig. 2a(i)), while *E. coli* containing Fe_3O_4 NPs showed a dark brown color (Fig. 2a(ii)). The colors of the *E. coli*, including the $AuFe_3O_4$ and $AgFe_3O_4$ NCs, were black (Fig. 2a(iii)) and ocher (Fig. 2a(iv)), respectively. After disrupting the cells,

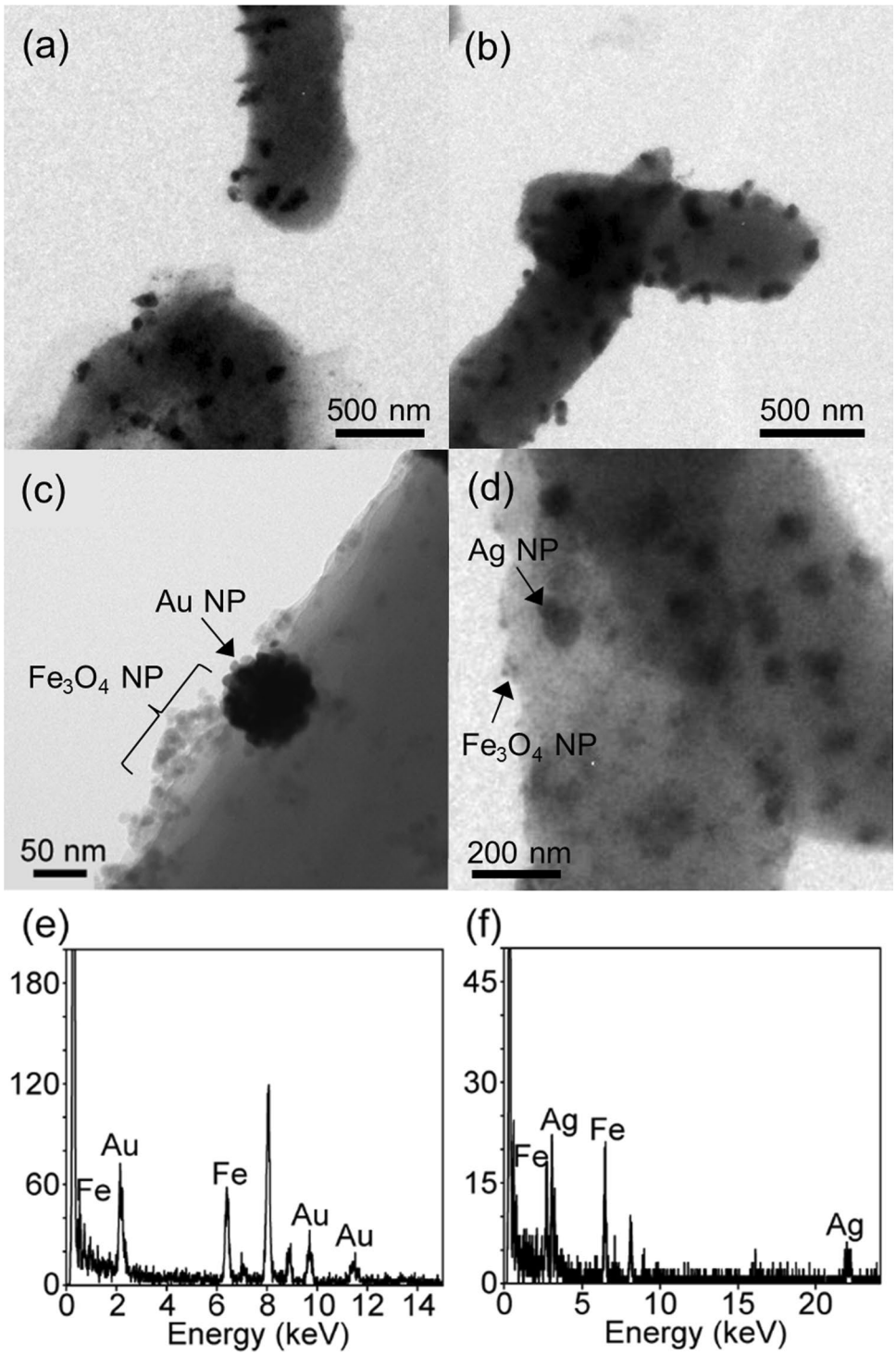

Fig. 1 TEM images of the recombinant *E. coli* containing **a** the $AuFe_3O_4$ and **b** $AgFe_3O_4$ NCs synthesized in vivo. Magnified TEM images of **c** the $AuFe_3O_4$ and **d** $AgFe_3O_4$ NCs in *E. coli*, and EDX spectra of *E. coli* containing **e** the $AuFe_3O_4$ and **f** $AgFe_3O_4$ NCs

the $AuFe_3O_4$ and $AgFe_3O_4$ NCs were purified from the cell debris by applying external magnets. The $AuFe_3O_4$ and $AgFe_3O_4$ NCs dispersed in DI water were seen dark purple (the left in Fig. 2b(i)) and yellowish-brown (the right in Fig. 2b(i)). Since pure Fe_3O_4 NP showed brown (Fig. S2), the NC colors ($AuFe_3O_4$ NCs; dark purple and $AgFe_3O_4$ NCs; yellowish-brown) indicated that Au or Ag conjugates to the Fe_3O_4 NPs. Moreover, the entirely dragged colored NCs by an external magnet demonstrated the conjugation among Fe_3O_4 NPs and Au/Ag ions (Fig. 2b(ii)). In the absorbance profiles of the NCs, the peak of the $AuFe_3O_4$ NCs at 550 nm proves the presence of Au NPs (Fig. 2c(i)), and the peak of the $AgFe_3O_4$ NCs at 410 nm indicates the existence of Ag NPs (Fig. 2c(ii)). We also measured the

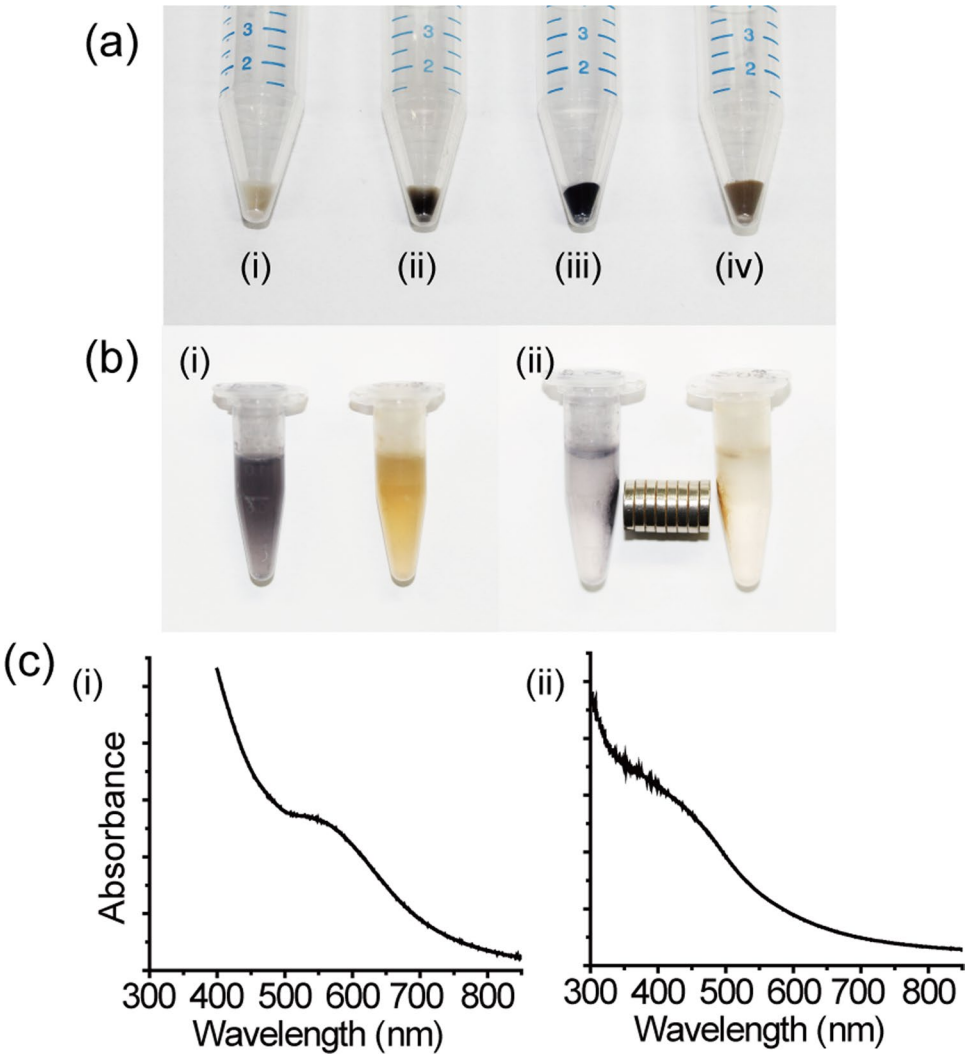

Fig. 2 **a** Digital images of the recombinant *E. coli* containing (i) nothing as a negative control, (ii) internalized the Fe_3O_4 NPs, (iii) the $AuFe_3O_4$, and (iv) $AgFe_3O_4$ NCs. **b** Digital images of (i) the purified solution of the $AuFe_3O_4$ (left) and $AgFe_3O_4$ NCs (right) and (ii) the NCs dragged by an external magnet. **c** Absorbance spectra of (i) the $AuFe_3O_4$ and (ii) $AgFe_3O_4$ NCs

absorbance of the iron oxide NPs as a negative control (Fig. S3). Therefore, all the observed results proved that the biosynthesized Au NPs and Ag NPs were conjugated to Fe_3O_4 NPs to form NCs.

Morphology of the biosynthesized NCs

The purified NCs from the cells were analyzed by TEM to observe the morphology (Fig. 3). In the images of the purified $AuFe_3O_4$ NCs, Au NPs showed a popcorn shape in black color (Fig. 3a–d), and the Fe_3O_4 NPs with grey color (around 10–15-nm diameter) were arranged around the Au NPs. As the Au concentration increased, the size of Au particles was measured as 33.3 ± 5.9 nm at 0.25 mM, 51.3 ± 7.2 nm at 0.5 mM, 83.0 ± 19.1 nm at 0.75 mM, and 111.1 ± 34.0 nm at 1.0 mM ($n \geq 20$, data presents mean ± standard deviation (SD)) (Fig. 3a–d and Table 1). In the purified $AgFe_3O_4$ NCs images, Ag NPs exhibited with black color, and the Fe_3O_4 NPs showed a grey color (Fig. 3e–h). In addition, the Ag NPs with a polygonal shape were observed around the Fe_3O_4 NPs, and the size of the Ag NPs enlarged with increasing Ag concentration from 0.5 to 2 mM. The Ag NP sizes were measured as 20.4 ± 5.4 nm at 0.5 mM, 29.5 ± 5.0 nm at 1.0 mM, 37.2 ± 9.3 nm at 1.5 mM, and 47.5 ± 18.2 nm at 2.0 mM ($n \geq 20$, mean ± SD) (Table 2). Consequently, the sizes of Au and Ag NPs in the NCs were controlled by the concentration of Au and Ag ions, respectively. The mass ratio of Au and Ag to Fe in the NCs also gradually increased as the concentration of Au and Ag ions increased (Table 3).

Crystallinity analysis of the biosynthesized NCs

The biosynthesized NCs were analyzed by XRD to demonstrate the NC biosynthesis (Fig. 4). First, Au and Ag NPs were synthesized using the same *E. coli*; then, crystallinities of the Au and Ag NPs were analyzed, respectively. Biosynthesized Au NPs showed four XRD peaks at 38.3°, 44.6°, 64.8°, and 77.8° (2θ) corresponding to the (111), (200),

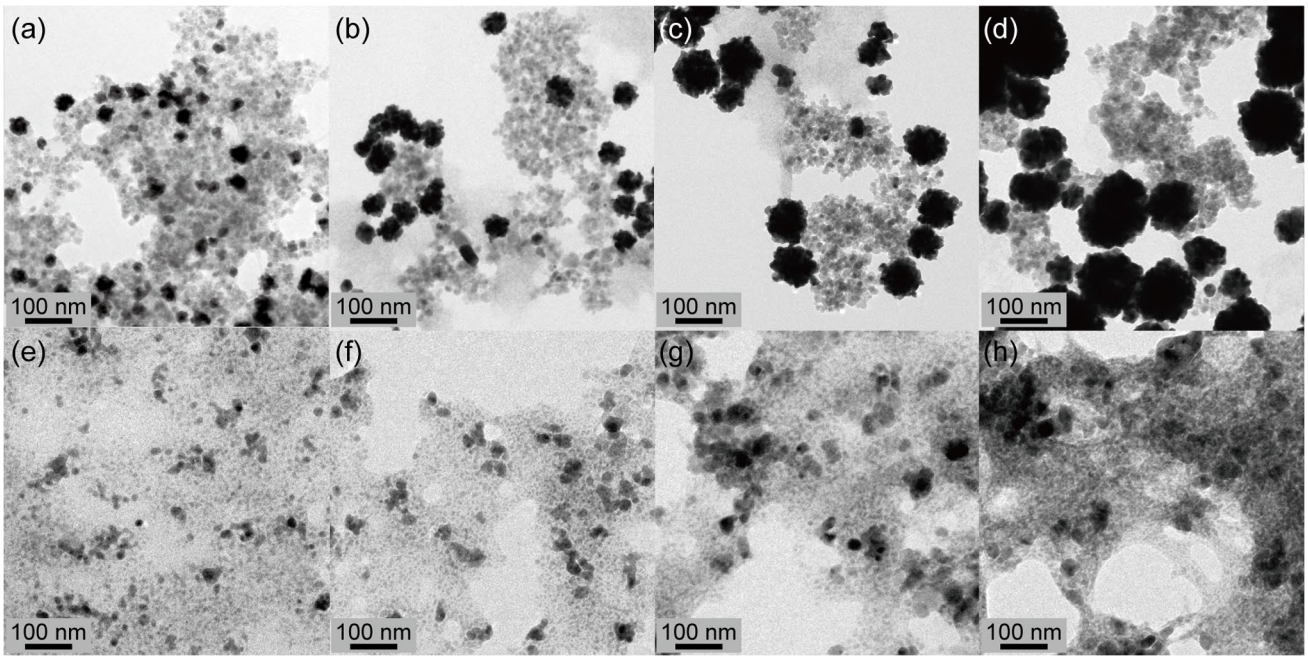

Fig. 3 TEM images of the purified $AuFe_3O_4$ NCs biosynthesized with different amount of Au ions, **a** 0.25, **b** 0.5, **c** 0.75, and **d** 1 mM. TEM images of the purified $AgFe_3O_4$ NCs biosynthesized with different amount of Ag ions, **e** 0.5, **f** 1, **g** 1.5, and **h** 2 mM

Table 1 The size of Au NPs in $AuFe_3O_4$ NCs according to Au ion concentration

Au ion concentration (mM)	Size of Au NP (nm)
0.25	33.3 ± 5.9
0.5	51.3 ± 7.2
0.75	83.0 ± 19.1
1.0	111.1 ± 34.0

Table 2 The size of Ag NPs in $AgFe_3O_4$ NCs according to Ag ion concentration

Ag ion concentration (mM)	Size of Ag NP (nm)
0.5	20.4 ± 5.4
1.0	29.5 ± 5.0
1.5	37.2 ± 9.3
2.0	47.5 ± 18.2

Table 3 The mass ratio of Au and Ag to Fe in the biosynthesized NCs

Au ion concentration (mM)	The mass ratio of Au/Fe	Ag ion concentration (mM)	The mass ratio of Ag/Fe
0.25	2.0	0.5	3.7
0.5	4.0	1.0	5.0
0.75	12.4	1.5	5.7
1.0	25.1	2.0	7.5

(220), and (311) planes, indicating pure Au NPs (JCPDS No. 04–0784) (Fig. 4a(i)). Fe_3O_4 NPs revealed that four peaks at 35.5°, 43.2°, 62.7°, and 74.2° (2θ) corresponding to the (311), (400), (440), and (533) planes (JCPDS file no: 19–0629) (Fig. 4a(ii) and b(ii)). In the patterns of the $AuFe_3O_4$ NC, both XRD patterns of the biosynthesized Au NPs (Fig. 4a(i)) and Fe_3O_4 NPs (Fig. 4a(ii)) were clearly observed (Fig. 4a(iii)).

The Ag NPs exhibited four main peaks at 38.2°, 46.2°, 67.4°, and 77.7° (2θ) corresponding to the (111), (200), (220), and (311) planes (JCPDS file no: 04–0783) (Fig. 4b(i)). Moreover, the XRD patterns of the biosynthesized Ag NPs (Fig. 4b(i)) and Fe_3O_4 NPs (Fig. 4b(ii)) were distinctly found in the patterns of the $AgFe_3O_4$ NCs (Fig. 4b(iii)). Therefore, the biosynthesis of $AuFe_3O_4$ and $AgFe_3O_4$ NCs was successfully proved through crystallinity analysis.

Prostate-specific antigen detection using the biosynthesized $AuFe_3O_4$ NCs

To demonstrate the practical use of the biosynthesized $AuFe_3O_4$ NCs, we performed the ELISA test to detect PSA using the $AuFe_3O_4$ NCs synthesized with 2 mM Au ions. In the reaction, first, "capture anti-PSA" was coated on a 96-well plate; then, different kinds of antigens such as PSA, CRP, and hCG were added into each well. Then, "detection anti-PSA" conjugated with the $AuFe_3O_4$ NCs was added,

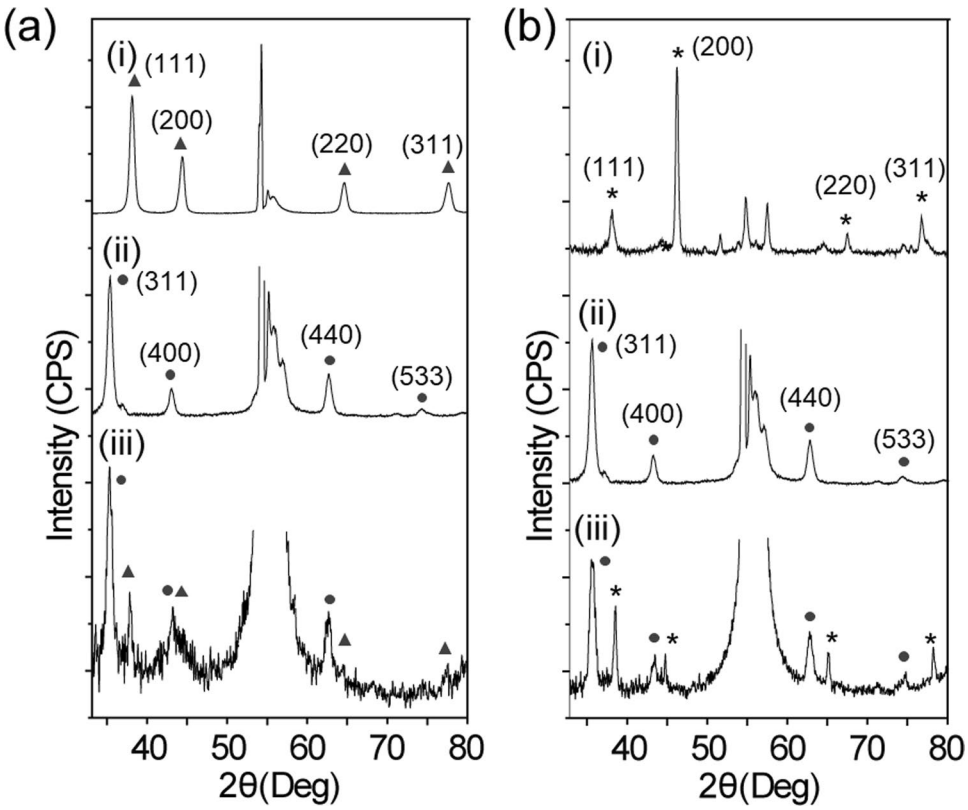

Fig. 4 **a** XRD patterns of (i) the Au NPs biosynthesized (no composites), (ii) the chemically synthesized Fe_3O_4 NPs, and (iii) the $AuFe_3O_4$ NCs biosynthesized. **b** XRD patterns of (i) the Ag NPs biosynthesized (no composites), (ii) the chemically synthesized Fe_3O_4 NPs, and (iii) the $AgFe_3O_4$ NCs biosynthesized. The peaks measured at 50 to 60° (2θ) are obtained from Si substrate

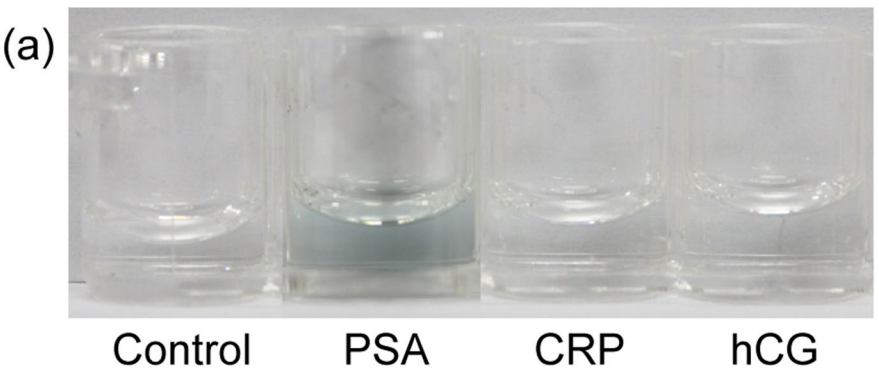

(b)

Bacteria	MIC values (mg/L)
Staphylococcus aureus	1.1
Listeria monocytogenes	0.07
Salmonella enterica	0.14

Fig. 5 **a** A digital image of ELISA test for PSA detection using the biosynthesized $AuFe_3O_4$ NCs. **b** Result of the MIC value from the antimicrobial test using the biosynthesized $AgFe_3O_4$ NCs

followed by TMB and hydrogen peroxide for colorimetric detection. Consequently, only the wells that contained the target PSA were specifically changed to blue (Fig. 5a). Therefore, we demonstrated that the $AuFe_3O_4$ NCs could be used as a target detecting probe in ELISA.

Antimicrobial test using the biosynthesized $AgFe_3O_4$ NCs

To evaluate the antimicrobial activity of the biosynthesized $AgFe_3O_4$ NCs, we measured MIC of the NCs to bacteria, *Staphylococcus aureus* and *Listeria monocytogenes* (Gram-positive bacteria), and *Salmonella enterica* (Gram-negative bacteria). The concentration of the NCs added to the bacteria was 0, 0.07, 0.14, 0.28, 0.56, 1.12, and 2.24 mg/L. After 1-day incubation at 37 °C, the MIC values were measured as 1.12, 0.07, and 0.14 mg/L for *Staphylococcus aureus*, *Listeria monocytogenes*, and *Salmonella enterica*, respectively (Fig. 5b). Thus, we could confirm that $AgFe_3O_4$ NC has strong antimicrobial activity.

Discussion

In this study, the recombinant *E. coli* internalized iron oxide NPs synthesized $AuFe_3O_4$ and $AgFe_3O_4$ NCs by adding Au and Ag ions, respectively. The *E. coli* have been utilized to synthesize various nanomaterials such as semiconducting, alkali-earth, magnetic, and noble metals (Park et al. 2010; Jung et al. 2012, 2018). Therefore, this biosynthesis system suggests that the *E. coli* in which iron oxide NPs are internalized can synthesize various NCs depending on the added ions in as well as the Au and Ag ions. Furthermore, this system has the potential to synthesize or discover various nanomaterials because other nanoparticles, as well as magnetic particles, can be used as internalizing materials. Since the reducing power required for biosynthesis is different for each ion, the culture conditions may be varied.

In a previous study, Ag-AuNR NCs were synthesized to a core–shell structure by the same recombinant *E. coli* (Jung et al. 2018). On the other hand, the $AuFe_3O_4$ and $AgFe_3O_4$ NCs in this study were synthesized in a network structure, not a core–shell structure (Fig. 3). Since the pattern of the XRD peaks and the lattice size are almost similar in Au and Ag, Ag can easily grow into a core–shell structure on Au nanorods (Chen et al. 2017; Prabhawathi et al. 2019). On the other hand, $AuFe_3O_4$ and $AgFe_3O_4$ NCs may be difficult to biosynthesize as a core–shell structure because Fe_3O_4 NP has an obviously different lattice and plane from Au and Ag NPs (Fig. 4) (Martínez-Mera et al. 2007). Therefore, since each metal has different crystallinity and electrical reducing power, different morphologies of NCs are synthesized depending on the metal used (Chang et al. 2016; Ma et al. 2019).

The network structure of iron oxide NCs has been reported in a previous study (Prucek et al. 2011; Bell et al. 2017). Prucek et al. reported $Ag@Fe_3O_4$ NCs synthesized in vitro using maltose and polyacrylate (Prucek et al. 2011). Ag ions were reduced and grown around Fe_3O_4 NPs by maltose, and the space between Ag and Fe_3O_4 NPs was controlled by polyacrylate. Bell et al. chemically synthesized iron oxide-Au nanocomposite (Bell et al. 2017). Citric acid-coated iron oxide NPs were used as a reducing agent that was added to Au ions for the synthesis of iron oxide-gold NCs. The structures of the iron oxide NCs reported in previous studies are similar to the morphology of the $AuFe_3O_4$ and $AgFe_3O_4$ NCs in this study. Thus, we could estimate the synthetic process of our $AuFe_3O_4$ and $AgFe_3O_4$ NCs (Fig. 6). As a first step, chemically synthesized Fe_3O_4 NPs were internalized into recombinant *E. coli*. Once the Fe_3O_4 NPs were coated and localized by PC and MT expressed,

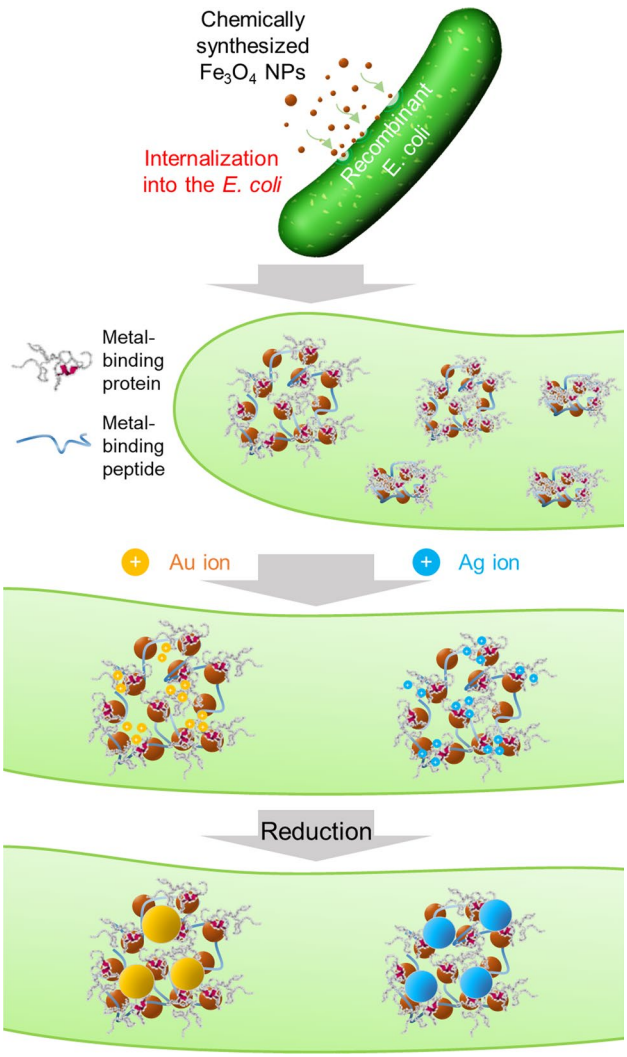

Fig. 6 Schematic illustration of the biosynthesis process of the $AuFe_3O_4$ and $AgFe_3O_4$ NCs

Au and Ag ions could be bound to thiol and carboxylate functional groups of PC and MT (Prucek et al. 2011). Then, PC and MT could reduce the ions around the Fe_3O_4 NPs. Consequently, PC and MT played two roles: a reducer of Au and Ag ions, and a spacer between the biosynthesized Au and Ag NPs, respectively.

Conventionally, biosynthesized nanomaterials have different shapes and sizes, making it difficult to use them for specific applications (Choi et al. 2018a, b; Ranoszek-Soliwoda et al. 2019). Moreover, nanomaterials synthesized in vivo are difficult to separate entirely from cells. To solve the problems of polydispersity and purification of nanomaterials previously mentioned, the NCs were synthesized based on chemically synthesized iron oxide NPs of uniform size. Although the iron oxide NCs synthesized in this study did not solve the polydispersity problem because they formed a network structure, those were entirely separated from cell debris by an external magnet and had relatively uniform properties. Therefore, $AuFe_3O_4$ NCs were used as target detection probes in the ELISA, and $AgFe_3O_4$ NCs were used as antimicrobial reagents, proving that the biosynthesized NCs can be utilized for practical applications. However, to apply the biosynthesized NCs to industry, it should have a high synthesis yield (Choi and Lee 2020). Since this study mainly focused on confirming the synthesizing potential of Au and Ag NCs and their properties, we plan to study the biosynthetic yield of the NCs and study methods to improve them as a follow-up study.

The advantage of using the $AuFe_3O_4$ NC as a target detection probe in ELISA is that, first, Au can be easily conjugated with antibodies without chemical linkers. Second, the magnetic property of the NCs facilitates the separation of the $AuFe_3O_4$ NC from unbound reagents. Third, the Fe_3O_4 NPs in the NCs can substitute horseradish peroxidase (HRP) in ELISA (Shin et al. 2017; Vallabani et al. 2017; Woo et al. 2013; Zhao et al. 2018). Thus, we conjugated the $AuFe_3O_4$ NCs to "detection anti-PSA" as an alternative to HRP. Au NP size used in ELISA is typically 10–80 nm (Guo et al. 2019; Lakshmipriya et al. 2016). In this study, the Au NP size of the NCs used for PSA detection was 111.1 ± 34.0 nm (at 1.0 mM of Au ion), slightly larger than the available size range. However, it partially belongs within the usable range and showed good target detection activity (Fig. 5a). Since the Au NP size of the NC synthesized at the other Au ion concentrations (0.25, 0.5, 0.75 mM) is also in the available range (Table 1), $AuFe_3O_4$ NCs are suitable for the use of biomedical applications. Moreover, since the network structure of the NCs can concentrate the Au NPs, the efficiency or sensitivity of the reaction can be improved.

The $AgFe_3O_4$ NCs have been employed for antimicrobial tests. In previous studies, antibiotic properties of Ag NPs have already been reported (Karthiga et al. 2018; Le Ouay and Stellacci 2015; Paladini and Pollini 2019; Panacek et al. 2006; Pazos et al. 2016). The network structure of the $AgFe_3O_4$ NCs, in which Fe_3O_4 NPs and Ag NPs are complexly connected by PC and MT (Fig. 3e–h), enhances the localized contact density among the cells and Ag NPs (Prucek et al. 2011; Trang et al. 2017; Zhang et al. 2016). Moreover, the NCs remain stable in an aqueous condition due to PC and MT (Markova et al. 2012; Prucek et al. 2011). Therefore, the antibacterial action of the $AgFe_3O_4$ NCs can be improved than the Ag NP solution. The obtained MIC values indicated that the biosynthesized $AgFe_3O_4$ NCs have more potent antimicrobial activity than the NCs reported in the previous studies (Liu et al. 2010; Markova et al. 2012; Prucek et al. 2011). Since the Ag NPs synthesized in vivo by strong reduction power from the *E. coli* were densely localized on the network of Fe_3O_4 NPs, the NCs could destroy bacteria intensively and effectively. The Ag NP size of the NC used in this antimicrobial test was 47.5 ± 18.2 nm synthesized at 2.0 mM Ag ion. Considering that the size range of Ag NPs generally used for the test is 10–50 nm, $AgFe_3O_4$ NC is suitable for the utilization of practical applications (Kubo et al. 2018; Ramalingmam et al. 2015). In conclusion, the biosynthesized NCs showed an efficient reaction in ELISA and antimicrobial test, respectively, showing the possibility that the nanomaterial synthesized in vivo can be used for practical applications.

Supplementary Information The online version contains supplementary material available at https://doi.org/10.1007/s00253-022-11779-4.

Acknowledgements We thank Dr. Yoojin Choi and Ms. Ji Hye Hyun for their helpful discussion.

Author contribution J.H.J. and M.J. performed experiments. J.H.J. and T.S.S. designed the study. J.H.J., T.S.S., and S.Y.L. wrote and revised the manuscript. All authors discussed the results and commented on the manuscript.

Funding The work was supported by the Bio and Medical Technology Development Program (Grant 2021M3A9I4022740) from the Ministry of Science and ICT (MSIT) through the National Research Foundation of Korea. This work was supported by the Engineering Research Center of Excellence Program of Korea Ministry of Science, ICT & Future Planning (MSIP)/National Research Foundation of Korea (NRF) (2021R1A5A6002853); National Research Foundation of Korea (NRF); and The Ministry of Science and ICT (MSIT) (2020R1A2C1003960). This research was supported by the Main Research Program (E0210701-01) of the Korea Food Research Institute funded by the Ministry of Science and ICT of South Korea.

Data availability Additional information is provided in the Supplementary Information.

Code availability Not applicable.

Declarations

Ethics approval Not applicable (no studies with human participants or animals were performed in this study).

Consent for publication All authors have read and approved the final manuscript.

Conflict of interest The authors declare no competing interests.

References

Bell G, Bogart LK, Southern P, Olivo M, Pankhurst QA, Parkin IP (2017) Enhancing the magnetic heating capacity of iron oxide nanoparticles through their postproduction incorporation into iron oxide-gold nanocomposites. Eur J Inorg Chem 18:2386–2395. https://doi.org/10.1002/ejic.201601432

Chang SH, Yang PY, Lai CM, Lu SC, Li GA, Chang WC, Tuan HY (2016) Synthesis of Cu/ZnO core/shell nanocomposites and their use as efficient photocatalysts. Cryst Eng Comm 18(4):616–621. https://doi.org/10.1039/C5CE01944C

Chen M, Zhang L, Gao M, Zhang X (2017) High-sensitive bioorthogonal SERS tag for live cancer cell imaging by self-assembling core-satellites structure gold-silver nanocomposite. Talanta 172:176–181. https://doi.org/10.1016/j.talanta.2017.05.033

Choi Y, Lee SY (2020) Biosynthesis of inorganic nanomaterials using microbial cells and bacteriophages. Nat Rev Chem 4:638–656. https://doi.org/10.1038/s41570-020-00221-w

Choi Y, Hwang JH, Lee SY (2018a) Recent trends in nanomaterials-based colorimetric detection of pathogenic bacteria and viruses. Small Methods 2(4):1700351. https://doi.org/10.1002/smtd.201700351

Choi Y, Park TJ, Lee DC, Lee SY (2018b) Recombinant *Escherichia coli* as a biofactory for various single- and multi-element nanomaterials. PNAS 115(23):5944–5949. https://doi.org/10.1073/pnas.1804543115

Cui W, Li J, Zhang Y, Rong H, Lu W, Jiang L (2012) Effects of aggregation and the surface properties of gold nanoparticles on cytotoxicity and cell growth. Nanomedicine 8(1):46–53. https://doi.org/10.1016/j.nano.2011.05.005

Guo S, Lakshmipriya T, Gopinath SC, Anbu P, Feng Y (2019) Complementation of ELISA and an interdigitated electrode surface in gold nanoparticle functionalization for effective detection of human blood clotting defects. Nanoscale Res Lett 14(1):1–10. https://doi.org/10.1186/s11671-019-3058-z

Jeong Y, Kook YM, Lee K, Koh WG (2018) Metal enhanced fluorescence (MEF) for biosensors: general approaches and a review of recent developments. Biosens Bioelectron 111:102–116. https://doi.org/10.1016/j.bios.2018.04.007

Jung JH, Park TJ, Lee SY, Seo TS (2012) Homogeneous biogenic paramagnetic nanoparticle synthesis based on a microfluidic droplet generator. Angew Chem Int Ed 51(23):5634–5637. https://doi.org/10.1002/anie.201108977

Jung JH, Lee SY, Seo TS (2018) In vivo synthesis of nanocomposites using the recombinant *Escherichia coli*. Small 14(42):1803133. https://doi.org/10.1002/smll.201803133

Karthiga P, Rajeshkumar S, Annadurai G (2018) Mechanism of larvicidal activity of antimicrobial silver nanoparticles synthesized using *Garcinia mangostana* bark extract. J Clust Sci 29(6):1233–1241. https://doi.org/10.1007/s10876-018-1441-z

Kubo AL, Capjak I, Vrček IV, Bondarenko OM, Kurvet I, Vija H, Ivask A, Kasemets K, Kahru A (2018) Antimicrobial potency of differently coated 10 and 50 nm silver nanoparticles against clinically relevant bacteria *Escherichia coli* and *Staphylococcus aureus*. Colloids Surf B 170:401–410. https://doi.org/10.1016/j.colsurfb.2018.06.027

Lakshmipriya T, Gopinath SC, Hashim U, Tang TH (2016) Signal enhancement in ELISA: Biotin-streptavidin technology against gold nanoparticles. J Taibah Univ Medical Sci 11(5):432–438. https://doi.org/10.1016/j.jtumed.2016.05.010

Le Ouay B, Stellacci F (2015) Antibacterial activity of silver nanoparticles: a surface science insight. Nano Today 10(3):339–354. https://doi.org/10.1016/j.nantod.2015.04.002

Liu Z, Zhao B, Shi Y, Guo C, Yang H, Li Z (2010) Novel nonenzymatic hydrogen peroxide sensor based on iron oxide-silver hybrid submicrospheres. Talanta 81(4–5):1650–1654. https://doi.org/10.1016/j.talanta.2010.03.019

Ma J, Du Q, Ge H, Zhang Q (2019) Fabrication of core–shell TiO_2@CuS nanocomposite via a bifunctional linker-assisted synthesis and its photocatalytic performance. J Mater Sci 54(4):2928–2939. https://doi.org/10.1007/s10853-018-3054-1

Markova Z, Siskova K, Filip J, Safarova K, Prucek R, Panacek A, Kolar M, Zboril R (2012) Chitosan-based synthesis of magnetically-driven nanocomposites with biogenic magnetite core, controlled silver size, and high antimicrobial activity. Green Chem 14(9):2550–2558. https://doi.org/10.1039/C2GC35545K

Martínez-Mera I, Espinosa-Pesqueira ME, Pérez-Hernández R, Arenas-Alatorre J (2007) Synthesis of magnetite (Fe3O4) nanoparticles without surfactants at room temperature. Mater Lett 61(23–24):4447–4451. https://doi.org/10.1016/j.matlet.2007.02.018

Paladini F, Pollini M (2019) Antimicrobial silver nanoparticles for wound healing application: progress and future trends. Materials 12(16):2540. https://doi.org/10.3390/ma12162540

Panacek A, Kvitek L, Prucek R, Kolar M, Vecerova R, Pizurova N, Sharma VK, Nevecna T, Zboril R (2006) Silver colloid nanoparticles: synthesis, characterization, and their antibacterial activity. J Phys Chem B 110(33):16248–16253. https://doi.org/10.1021/jp063826h

Park TJ, Lee SY, Heo NS, Seo TS (2010) In vivo synthesis of diverse metal nanoparticles by recombinant *Escherichia coli*. Angew Chem Int Ed 49(39):7019–7024. https://doi.org/10.1002/anie.201001524

Pazos E, Sleep E, Rubert Pérez CM, Lee SS, Tantakitti F, Stupp SI (2016) Nucleation and growth of ordered arrays of silver nanoparticles on peptide nanofibers: hybrid nanostructures with antimicrobial properties. J Am Chem Soc 138(17):5507–5510. https://doi.org/10.1021/jacs.6b01570

Prabhawathi V, Sivakumar PM, Boobalan T, Manohar CM, Doble M (2019) Design of antimicrobial polycaprolactam nanocomposite by immobilizing subtilisin conjugated Au/Ag core-shell nanoparticles for biomedical applications. Mater Sci Eng: C 94:656–665. https://doi.org/10.1016/j.msec.2018.10.020

Prucek R, Tucek J, Kilianova M, Panacek A, Kvitek L, Filip J, Kolar M, Tomankova K, Zboril R (2011) The targeted antibacterial and antifungal properties of magnetic nanocomposite of iron oxide and silver nanoparticles. Biomaterials 32(21):4704–4713. https://doi.org/10.1016/j.biomaterials.2011.03.039

Ramalingmam P, Muthukrishnan S, Thangaraj P (2015) Biosynthesis of silver nanoparticles using an endophytic fungus, *Curvularialunata* and its antimicrobial potential. J Nanosci Nanoeng 1(4):241–247

Ranoszek-Soliwoda K, Tomaszewska E, Małek K, Celichowski G, Orlowski P, Krzyzowska M, Grobelny J (2019) The synthesis of monodisperse silver nanoparticles with plant extracts. Colloids Surf B 177:19–24. https://doi.org/10.1016/j.colsurfb.2019.01.037

Shin HY, Kim BG, Cho S, Lee J, Na HB, Kim MI (2017) Visual determination of hydrogen peroxide and glucose by exploiting

the peroxidase-like activity of magnetic nanoparticles functionalized with a poly(ethylene glycol) derivative. Microchim Acta 184(7):2115–2122. https://doi.org/10.1007/s00604-017-2198-z

Trang VT, Van Quy N, Huy TQ, Thuy NT, Tri DQ, Cuong ND, Tuan PA, Van Tuan H, Le A-T, Phan VN (2017) Functional iron oxide–silver hetero-nanocomposites: controlled synthesis and antibacterial activity. J Electron Mater 46(6):3381–3389. https://doi.org/10.1007/s11664-017-5314-2

Vallabani NVS, Karakoti AS, Singh S (2017) ATP-mediated intrinsic peroxidase-like activity of Fe3O4-based nanozyme: one step detection of blood glucose at physiological pH. Colloids Surf B Biointerfaces 153:52–60. https://doi.org/10.1016/j.colsurfb.2017.02.004

Woo MA, Kim MI, Jung JH, Park KS, Seo TS, Park HG (2013) A novel colorimetric immunoassay utilizing the peroxidase mimicking activity of magnetic nanoparticles. Int J Mol Sci 14(5):9999–10014. https://doi.org/10.3390/ijms14059999

Yu X, Marks TJ, Facchetti A (2016) Metal oxides for optoelectronic applications. Nat Mater 15(4):383–396. https://doi.org/10.1038/nmat4599

Zhang HZ, Zhang C, Zeng GM, Gong JL, Ou XM, Huan SY (2016) Easily separated silver nanoparticle-decorated magnetic graphene oxide: Synthesis and high antibacterial activity. J Colloid Interface Sci 471:94–102. https://doi.org/10.1016/j.jcis.2016.03.015

Zhang J, Wang L, Zhang B, Zhao H, Kolb U, Zhu Y, Liu L, Han Y, Wang G, Wang C, Su DS, Gates BC, Xiao FS (2018) Sinter-resistant metal nanoparticle catalysts achieved by immobilization within zeolite crystals via seed-directed growth. Nat Catal 1(7):540–546. https://doi.org/10.1038/s41929-018-0098-1

Zhao J, Dong WF, Zhang XD, Chai HX, Huang YM (2018) FeNPs@Co3O4 hollow nanocages hybrids as effective peroxidase mimics for glucose biosensing. Sens Actuators B Chem 263:575–584. https://doi.org/10.1016/j.snb.2018.02.151